Catalysis Letters
https://doi.org/10.1007/s10562-019-02822-7

Influence of Support Acidity of Pt/Nb_2O_5 Catalysts on Selectivity of CO_2 Hydrogenation

Si Bui Trung Tran[1] · Hanseul Choi[1,2] · Sunyoung Oh[1,2] · Jeong Young Park[1,2]

Received: 10 March 2019 / Accepted: 2 May 2019

Abstract

In solid acid catalysis, understanding the impact of support acidity on catalytic performance has remained a controversial issue. The selected catalytic systems often rely on mixing different substances to control the degree of acidity, which in turn, also modifies other parameters in the system, making it challenging to perform a definitive study. To specifically investigate the role of support acidity, we performed a systematic study employing Nb_2O_5 as the catalyst support, which acidity can be controlled by calcination. The catalytic behavior of the fabricated Pt/Nb_2O_5 catalysts was evaluated using CO_2 hydrogenation to methanol (MeOH) and dimethyl ether (DME). An increase in the acidity of the support resulted in an improvement in the CO_2 conversion owing to the strong interaction between the Pt and the catalyst support, but it was detrimental for the production of MeOH because of the unfavorable adsorption of CO_2 molecules and the formation of carbon-containing species on the surface of the support with high acidity. DME selectivity was enhanced with an increase in catalyst acidity, confirming the role of solid acids for the production of DME from CO_2 reduction.

Electronic supplementary material The online version of this article (https://doi.org/10.1007/s10562-019-02822-7) contains supplementary material, which is available to authorized users.

Extended author information available on the last page of the article

Published online: 16 May 2019

Graphical Abstract

By controlling the calcination temperature of Nb_2O_5, tunable support acidity was obtained. CO_2 conversion increased while the selectivity of methanol and dimethyl ether decreased with increasing support acidity.

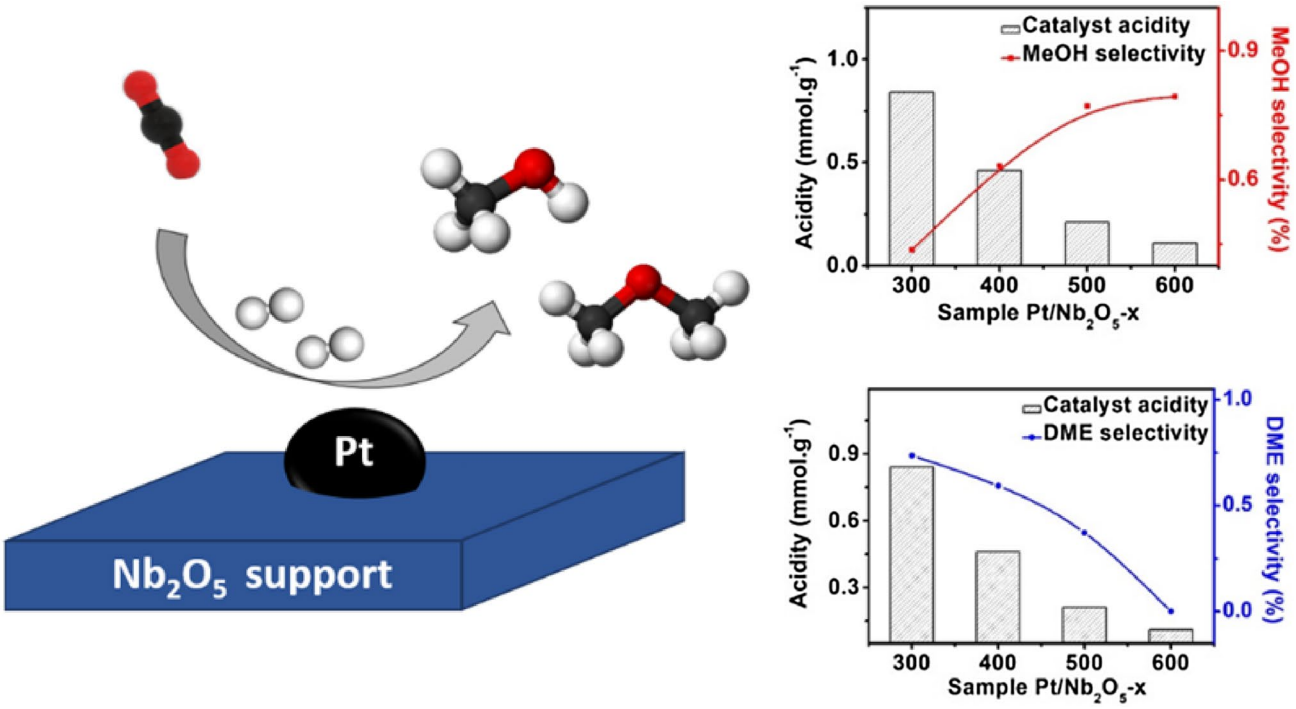

Keywords Pt-based catalyst · Niobium oxide · Support acidity effect · CO_2 hydrogenation · Methanol synthesis · Dimethyl ether synthesis

1 Introduction

Acid catalysis is known as unique chemistry that relies on charge transport via protons, which determines the generation of ionic intermediates in a specific pathway during the reaction, resulting in the improvement of rate and selectivity [1]. Solid acids, a combination of both acid catalysis and heterogeneous catalysis, not only catalyze a wide range of chemical reactions but also provide many of the advantages of a heterogeneous catalytic system, such as easy separation of products, catalyst reusability, and high purity of the product; therefore, they have been employed for a variety of industrial applications [2–4]. Solid acid catalysis has many similarities with the electronic effect of the strong metal–support interaction phenomenon, which originates from charge transfer between the metal and the catalyst support and has been the focus of much attention because of its enormous influence on catalytic properties [5, 6]. A deep understanding of the influence of acidity on catalytic performance plays a vital role in the design and development of efficient catalyst systems. To fulfill this goal, typical studies comparing catalysts with different acidic levels have been performed.

The strategy for controlling the acidity of catalysts generally depends on the blend of metal oxides, in which each one possesses either acidic or basic properties. For instance, to investigate the effect of the acidic properties of the catalyst support on catalytic selectivity and activity for hydrogenation isomerization of methylcyclopentale, Na et al. [7] controlled the acidity of a zeolite by modifying the Al_2O_3/SiO_2 ratio during postdealumination. Likewise, Silva et al. [8] functionalized different amounts of Nb_2O_5 to SBA-15 to control the acidity of the catalysts for acid-catalyzed esterification of propanoic acid with methanol. Esterification activity was found to be directly proportional to the Brønsted/Lewis acid ratio. This strategy, however, has the drawback of only considering controlling the acidity, while neglecting other factors that may affect the catalytic performance. When two or more metal oxides are mixed, the acidity of the system is tuned, but other properties are also modified that depend on the nature of each metal oxide (e.g. physicochemical or electrical properties) or the nature of mixing (e.g. doping, chemical bonding, or physical mixing). As a result,

these studies may lead to misleading conclusions about the influence of acidity. Therefore, for specifically investigating the role of acidity on catalytic performance, selecting catalytic systems that only tune catalyst acidity while keep other properties constant is crucial. Thus, the use of a mono metal oxide would be an appropriate approach since it eliminates the inherent disadvantages of mixing metal oxides.

Niobium oxide is among the most applicable solid acids for many reactions such as alkylation, esterification, dehydration, and hydrolysis [9–11]. Niobium oxide has been commonly used as the support along with metal nanocatalysts for the study of the strong metal–support interaction [12, 13]. Amorphous niobium oxide is mainly comprised of distorted NbO_6 octahedra and NbO_4 tetrahedra as the structural units, in which the Nb–O bonds are highly polarized. Thus, the metal oxide possesses both surface OH groups functionalized as Brønsted acidic sites on the NbO_6 octahedra and Lewis acidic sites on the NbO_4 tetrahedra [14, 15]. Depending on the heat treatment conditions, amorphous Nb_2O_5 transforms to different polyhedral structures and phases (i.e. pseudohexagonal niobium oxide (TT-Nb_2O_5) at 300–500 °C, orthorhombic niobium oxide (T-Nb_2O_5) at 700–800 °C, and monoclinic niobium oxide (H-Nb_2O_5) at temperatures over 1000 °C), which consequently leads to changes in the level of acidity [16]. According to infrared (IR) adsorbed pyridine analysis, the number of both the Lewis and Brønsted acidic sites of Nb_2O_5 drops significantly when the calcination temperature increases from 300 to 600 °C [17]. This interesting property provides a method for manipulating the acidic sites of the Nb_2O_5 based on changing the heat treatment conditions.

Direct production of MeOH and DME from CO_2 hydrogenation has long aroused great interest. MeOH is among the most prevalent starting chemicals for the synthesis of different organic materials, while DME has been considered as a potential alternative for diesel oil because of its superior combustion properties [18, 19]. With regards to environmental aspects, CO_2 capture and utilization by means of its conversion to other useful chemicals helps reduce the greenhouse gas effect. Despite a decent amount of research devoted to the study of the effect of acidity/basicity on the catalytic performance of this reaction, the conclusions remain inconsistent because of the different catalytic systems used as well as the lack of direct observations. Basic sites, which are controlled by introducing basic metal oxides or alkaline earth oxides into catalysts, were found to promote the selectivity of CO_2 hydrogenation to MeOH synthesis [20–22]. The enhancement of both the metallic surface area and the adsorption ability of the acidic CO_2 molecule on the basic catalyst surface was claimed to be the main reason for the selectivity. On the other hand, Hengne et al. [23] introduced Ga into Cu supported on SBA-15 catalysts and found that the support acidity enhanced the activity and selectivity for CO_2 hydrogenation to MeOH production by promoting the formation of smaller Cu particles and higher metal surface area. Obviously, using mixtures of different metal oxides to investigate the impact of acidity/basicity on the reaction can result in ambiguous outcomes by introducing external elements into the catalyst system that may contribute to changes in catalytic behavior.

Earlier studies report the CO_2 hydrogenation reaction with Nb_2O_5 as a support. Silva et al. measured catalytic activity of Cu/ZnO catalysts supported on Nb_2O_5 for CO_2 hydrogenation to methanol and DME [24]. They controlled the total acidity including the medium and strong acid sites by using different synthesis methods for Nb_2O_5. In the catalytic reaction, Nb_2O_5 with a relatively low total acidity showed 100% methanol selectivity, while the other showed 95% methanol selectivity and 5% DME selectivity at 270 °C. This result clearly illustrates the effect of acidity on selectivity for CO_2 hydrogenation reactions. Gnanakumar also studied the CO_2 hydrogenation reaction with Nb_2O_5 as the support [25]. Here, they also controlled acidity by changing the calcination temperature, and they conclude that the calcination temperature affects acidic density and the strength of the acid sites and strong acidic sites might favorable in the CO_2 hydrogenation reaction.

Herein, we employed Nb_2O_5 as the catalyst support to systematically investigate the effect of acidity on the catalytic activity and selectivity of direct CO_2 hydrogenation to MeOH and DME. The acidity of the fabricated Nb_2O_5 supports was controlled by changing the calcination temperature. To focus on the impact of the catalyst support on catalytic performance, Pt metal was selected for this study because Pt has not been reported to promote MeOH and DME production [26, 27]; hence, any influence on the catalytic activity originates solely from changes in the acidic sites on the catalyst supports. Platinum was impregnated onto the Nb_2O_5 supports and the catalysts were characterized using powder X-ray diffraction (XRD), X-ray photoelectron spectroscopy (XPS), the Brunauer–Emmett–Teller (BET) method, transmission electron microscopy (TEM), X-ray fluorescence (XRF), CO_2 temperature-programmed desorption (CO_2-TPD), and NH_3 temperature-programmed desorption (NH_3-TPD). In situ diffuse reflectance infrared Fourier transform (DRIFT) of CO_2 hydrogenation to MeOH and DME was carried out using the synthesized catalysts and the dependence of the catalytic performance on the support acidity was discussed.

2 Experimental

2.1 Preparation of Catalysts

Niobium oxide supports were synthesized using the following procedure: First, 10 g of $NbCl_5$ was slowly added

to 60 mL of ethanol while stirring to prevent an increase in temperature. The solution was kept at 40 °C while stirring until the ethanol evaporated completely. The remaining solid was dried in an oven overnight at 100 °C and was then calcined at different temperatures for 5 h. The samples after calcination were denoted as Nb_2O_5-300, Nb_2O_5-400, Nb_2O_5-500, and Nb_2O_5-600, where the final number is the calcination temperature.

The platinum-based catalysts were prepared using the impregnation method with H_2PtCl_6 as the precursor. In a typical synthesis, the Pt precursor solution was prepared by fully dissolving H_2PtCl_6 in water. The solution was added to 1000 mg of the synthesized Nb_2O_5, targeting a platinum loading of 3 wt%. Subsequently, the mixture was heated to 80 °C while stirring and kept at this temperature until the solvent evaporated completely. The remaining powder was dried in an oven overnight at 110 °C and reduced at 300 °C under a flow of H_2 at 50 mL min^{-1} for 2 h for the characterization. The Pt-based catalysts were denoted as Pt/Nb_2O_5-x, where x (i.e. 300, 400, 500, and 600) is the calcination temperature of the Nb_2O_5 support.

2.2 Characterization of the Catalysts

XRD patterns were collected to confirm the structures of the synthesized catalysts using a D/MAX-2500 Rigaku (at 40 kV and 300 mA) that scanned 2θ values between 20° and 65°. TEM images were obtained using a TECNAI F30 transmission electron microscope operating at an acceleration voltage of 300 kV. N_2 adsorption measurements were carried out at − 196 °C using a Micromeritics TriStar II 3020 V1.03 Analyzer and the surface areas were calculated using the BET method. The amount of Pt loading on each sample was measured by XRF in a Rigaku ZSX Primus II spectrometer containing a Rh-anode tube as the X-ray source. The oxidation states of the Pt were evaluated using a VG Scientific Sigma Probe XPS system equipped with an Al Kα X-ray source (1486.3 eV) under ultra-high vacuum at 10^{-10} Torr.

TPD of the as-prepared catalysts was performed using a Micromeritics BELCAT-B (BEL Japan Inc.) instrument with a thermal conductivity detector (TCD). For the CO_2-TPD experiment, 100 mg of the Pt–based catalysts were reduced at 300 °C under H_2 for 2 h, and then kept at 300 °C for 1 h under He gas to clean the catalyst surface. Subsequently, the samples were cooled down to 50 °C and saturated in flowing CO_2 (50 mL min^{-1}) for 1 h, followed by flushing in He for 30 min. The CO_2-TPD measurements were performed at temperatures of 50–350 °C with a heating rate of 10 °C min^{-1} under a continuous flow of He carrier gas. For the NH_3-TPD experiments, 100 mg of the Pt-based catalysts were reduced at 300 °C under H_2 for 2 h, followed by heat treatment at 300 °C for 1 h under He gas. The samples were then cooled down to 100 °C and exposed to NH_3 (50 mL min^{-1}) for 1 h. After saturation, the samples were purged with He for 30 min to remove any physisorbed NH_3. The NH_3-TPD measurements were conducted at 100–420 °C with a heating rate of 10 °C min^{-1}. Metal dispersion on the samples was obtained by using the same Micromeritics BELCAT-B (BEL Japan Inc.) instrument operated in the CO pulse chemisorption regime with a stoichiometry factor of Pt:CO = 1:1. The samples were pretreated at 300 °C under H_2 flow (50 mL min^{-1}) for 2 h. The measurement was carried out at 50 °C using a gas pulse composed of 10% CO gas balanced with He.

The DRIFT experiments were carried out using a Fourier-transform infrared spectrometer (Carry 660, Agilent) with the detailed equipment setup and experimental procedure described elsewhere [28]. In short, the catalysts were pretreated under 5% H_2/Ar flow at 300 °C for 2 h and then purged with a flow of He to cool down to 100 °C. After purging with He gas at 100 °C for 30 min, a background spectrum was recorded for further analysis. A feed gas composed of 30% H_2, 10% CO_2, and 60% He was then introduced into the IR cell with a total flow rate of 100 mL min^{-1}. The catalysts were heated linearly to 300 °C at 5 °C min^{-1} and the IR spectra were collected at different temperatures.

2.3 Evaluation of Catalytic Activity

The catalytic performance for MeOH and DME synthesis from CO_2 hydrogenation was carried out in a fixed bed tubular stainless steel reactor. Typically, 200 mg of each Pt/Nb_2O_5-x catalyst was reduced under atmospheric pressure with flowing H_2 (50 mL min^{-1}) at 300 °C for 2 h. After reduction, the reactor temperature was cooled to 150 °C under flowing He; subsequently, a gas mixture composed of CO_2, H_2, and N_2 started flowing into the reactor. The volume ratio of CO_2:H_2:N_2 was 22:68:10, with N_2 used as the internal standard gas. The total flow rate of the mixed gas was set at 100 mL min^{-1}, as calibrated and determined using Brooks 5850 series mass flow controllers. The pressure inside the reactor was adjusted to 5 bar until a steady-state condition was reached. Afterwards, the reaction temperature was increased and data were collected from 180 to 300 °C at 20 °C intervals for all the CO_2 hydrogenation experiments. The gaseous products were analyzed using a gas chromatography iGC 7200 (DS Science) that was equipped with a thermal conductivity detector (TCD) and a Carbosphere column to analyze H_2, CO, CO_2, and N_2, and with a flame ionization detector (FID) and a HP-plot/Q column to analyze the MeOH and DME. The activity–selectivity data were calculated by both the internal standard and mass-balance methods [29] at the steady state values that were determined by the average of the three different analyses.

3 Results and Discussion

3.1 Characterization of the Synthesized Pt-Based Catalysts

The surface area and amount of Pt loading of the synthesized Pt-based catalysts were assessed using N_2 adsorption–desorption and XRF analyses, respectively. As seen in Table 1, all the catalysts showed similar surface areas and Pt weight proportions, suggesting that these factors did not play a significant role in the comparison of catalytic activity. However, Pt dispersion, which was evaluated using the CO chemisorption method, showed a downward trend with increasing Nb_2O_5 calcination temperature. Among the catalysts, Pt/Nb_2O_5-300 possessed the highest Pt dispersion (7.17%) whereas Pt/Nb_2O_5-600 had the lowest value (4.82%). The data suggested that although the Pt loadings were similar for all the catalysts, the dispersion and size distribution of the Pt nanoparticles (NPs) could cause a difference in the behavior of the active Pt sites. As the metal active site has a close relationship with the morphological structure, TEM analysis was employed to further investigate the morphology of the fabricated Pt-based catalysts.

Figure 1 shows TEM images of the Pt/Nb_2O_5-x catalysts and their corresponding particle size distributions. HR-TEM images of the random small dark spots revealed a lattice fringe of 0.225 nm, typical of the Pt (111) surface (JCPDS card no. 65-2868), which confirmed that these dark spots are Pt NPs. In all the samples, Pt NPs were distributed homogeneously on the surface of the supports. However, the TEM images show that the Pt particle sizes were not similar. To study the size distribution of the Pt NPs in each catalyst, a statistical size measurement of more than 200 particles was carried out (Fig. 1). In general, the sizes of the Pt NPs in all the samples fell roughly within the range of 1.5–5 nm, with the average size increasing as the Nb_2O_5 supports were treated at higher temperatures. Particularly, the Pt/Nb_2O_5-600 catalyst had an additional size distribution region of 6 to 10 nm. Based on the TEM observations, it was suggested that the increasing calcination temperature of the Nb_2O_5 supports led to the increase in Pt particle size, thus resulting in a decrease in the Pt active surface area, as observed from the CO chemisorption analysis.

The crystalline structures of the synthesized materials were studied using XRD. Figure 2 shows XRD patterns of the as-prepared Nb_2O_5 at different calcination temperatures and of the Pt-based catalysts after reduction at 300 °C under H_2 flow. As seen in Fig. 2a, the Nb_2O_5 samples calcined at 300 and 400 °C only exhibited a broad 2θ peak at 25°, which is attributed to amorphous niobia. However, after being loaded with Pt and reduced under H_2, these samples exhibited the typical crystalline hexagonal phase TT-Nb_2O_5 (JCPDS 28-0317), as shown in Fig. 2b. A similar evolution of the crystallinity has been observed in the case of a Ni/Nb_2O_5 hybrid before and after reduction in H_2 [30]. The explanation for this phenomenon is not yet clear, but a reasonable description is that the presence of metals like Ni and Pt under reducing conditions may assist in converting the flexible structure of amorphous Nb_2O_5 to a more stable crystalline form by reconfiguring the Nb_2O_5 network. The Nb_2O_5-500 and Pt/Nb_2O_5-500 samples showed similar peaks that were well defined to the (001), (100), (101), (002), (110), and (102) crystalline planes of hexagonal phase TT-Nb_2O_5. On the other hand, the Nb_2O_5-600 and Pt/Nb_2O_5-600 samples exhibited additional peaks (marked as asterisks in Fig. 2a) that were typically indexed to the orthorhombic phase of Nb_2O_5 (JCPDS 27-1003). The increase in crystallinity as well as the transformation of the phase structure of Nb_2O_5 with rising temperature, as observed in the XRD data in this work, is consistent with the literature [31, 32]. It is worth noting that Pt diffraction peaks were not clearly detected in the XRD patterns in Fig. 2b, which was most likely because of low Pt loading on the supports and the relatively small Pt NP size.

To properly evaluate the influence of acidity on catalytic performance, we determined the acidic level of the synthesized Pt-based catalysts instead of the niobium oxide materials. The strength and concentration of the acidity existing on the catalyst supports were estimated by TPD of NH_3. Due to NH_3 being basic, its ability to selectively adsorb on different sites (weak, medium, and strong), and its small kinetic diameter (0.26 nm), NH_3 is used as a probe molecule to provide comparative details about the surface acidity of the catalysts. Figure 3a showed the results of the NH_3-TPD analysis of the synthesized Pt-based catalysts at

Table 1 Characterization of surface area, Pt wt% loading, Pt dispersion, amount of desorbed CO_2, and Pt^0 $4f_{7/2}$ peak position of the synthesized Pt/Nb_2O_5-x catalysts

Samples	BET (m^2 g^{-1})	Pt wt (%)	Pt dispersion (%)	Desorbed CO_2 (mmol g^{-1})	Pt^0 $4f_{7/2}$ peak position (eV)
Pt/Nb_2O_5-300	3.58	3.41	7.17	0.06	71.53
Pt/Nb_2O_5-400	2.98	3.31	6.45	0.10	71.21
Pt/Nb_2O_5-500	2.52	3.32	6.01	0.11	71.05
Pt/Nb_2O_5-600	2.90	3.38	4.82	0.18	71.03

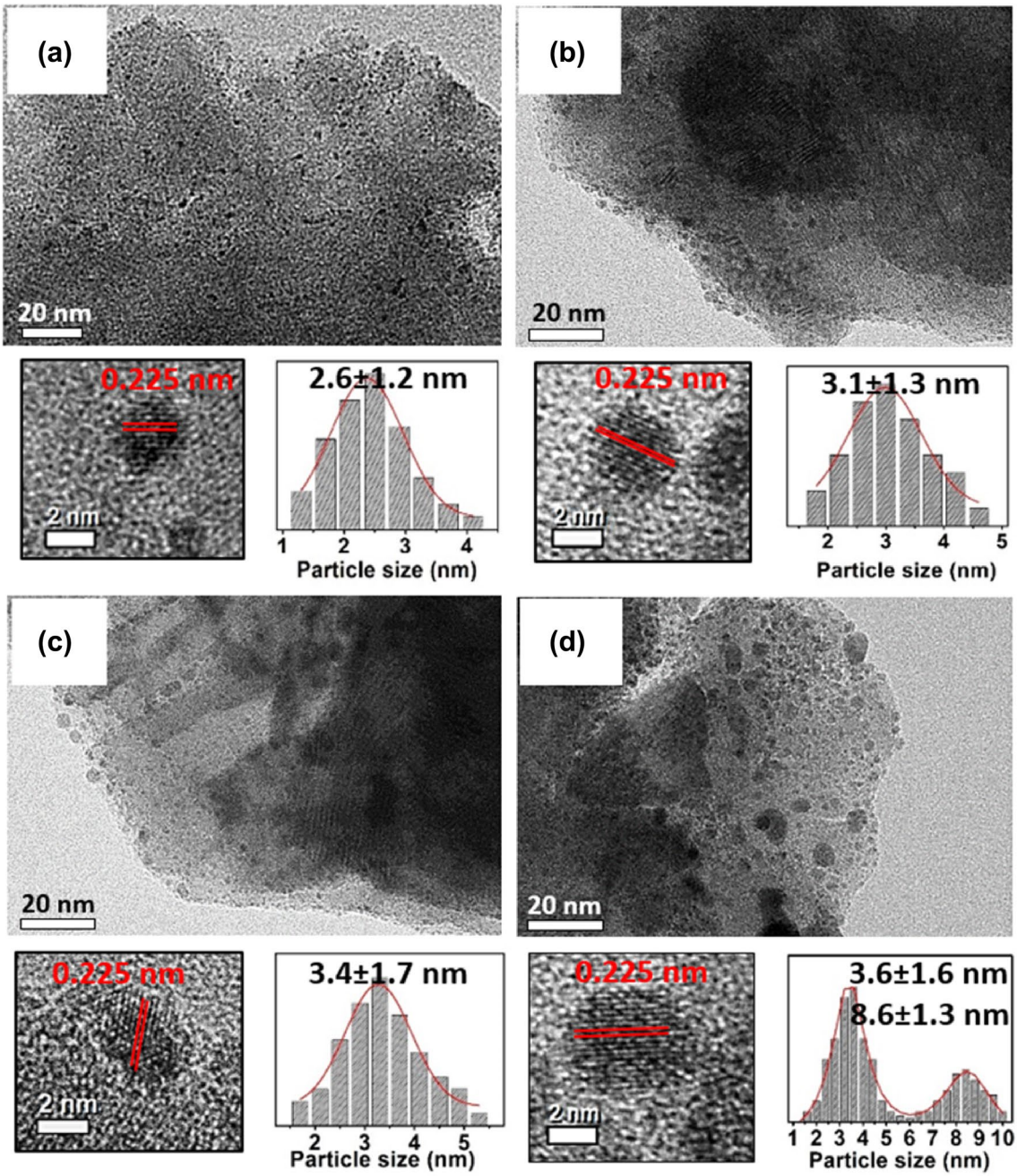

Fig. 1 TEM and HR-TEM images of the synthesized **a** Pt/Nb_2O_5-300, **b** Pt/Nb_2O_5-400, **c** Pt/Nb_2O_5-500, and **d** Pt/Nb_2O_5-600 catalysts and their corresponding particle size distributions

temperatures of 100–420 °C. All the catalysts exhibited a broad peak composed of two desorption signals ranging from 100 to 220 °C and from 230 to 400 °C, which were attributed to the desorption from weak and medium acidic sites, respectively [33]. The area of these peaks decreased as the calcination temperature of the support Nb_2O_5 increased. The peak area is an important parameter for evaluating acidity because it represents the concentration of the acidic sites on the samples. As depicted in Fig. 3b, the concentrations of the acidic sites on the Pt/Nb_2O_5-300, Pt/Nb_2O_5-400, Pt/Nb_2O_5-500, and Pt/Nb_2O_5-600 catalysts determined by the uptake of NH_3 were 0.65, 0.39, 0.19, and 0.11 mmol g^{-1}, respectively. Since the acidity of the Nb_2O_5 decreases with increasing calcination temperature [17], the results suggest that growing Pt NPs on Nb_2O_5 supports produced a similar trend in the change in acidity as a function of calcination temperature as that of Nb_2O_5. It is worth mentioning that the presence of surface acidity could significantly affect the

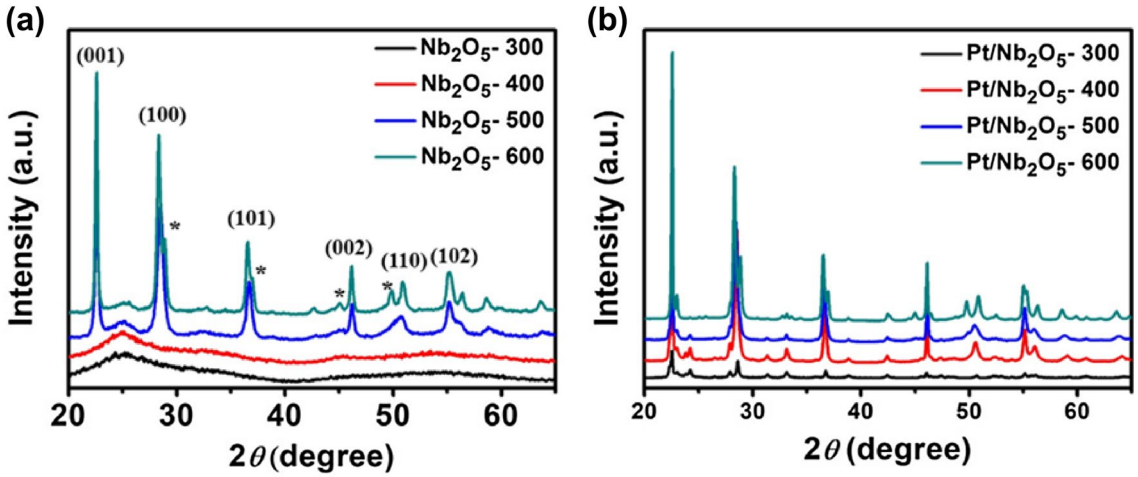

Fig. 2 XRD patterns of the synthesized **a** Nb_2O_5 materials, and **b** Pt/Nb_2O_5-x catalysts

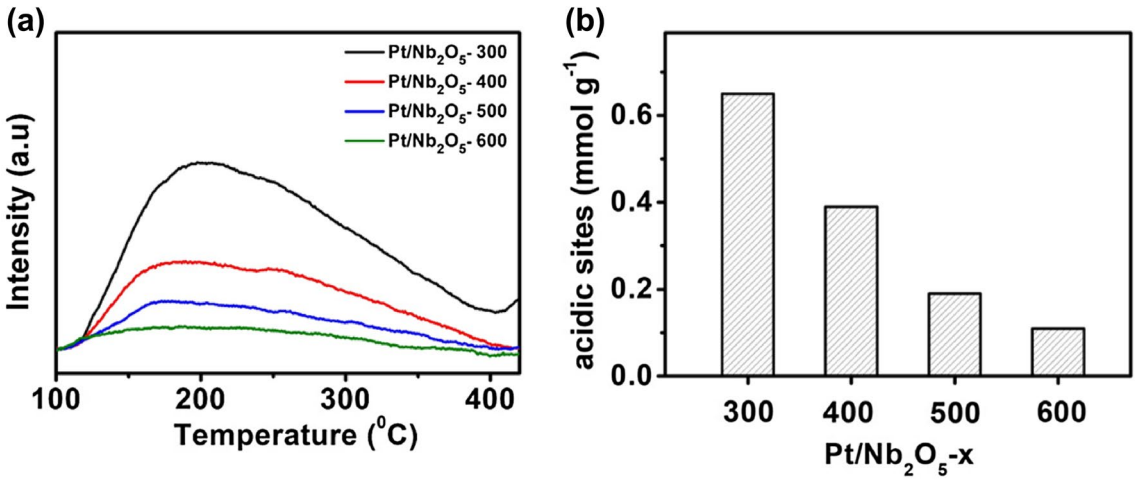

Fig. 3 **a** NH_3-TPD evaluations of the Pt/Nb_2O_5-x catalysts at temperatures of 100–420 °C. **b** The total number of acidic sites of the catalysts based on NH_3-TPD analysis

behavior of the Pt size distribution of the catalysts. During the impregnation process, the acidic sites of the catalyst support play a role as anchor sites for the nucleation and growth of the Pt NPs. More acidic sites led to the formation of more Pt NPs, which resulted in smaller NP sizes and increased particle dispersion. Thus, the trend of the change in acidity obtained from the NH_3-TPD analysis was consistent with the Pt size distribution observed from the TEM images.

Because CO_2 is the main reactant in the CO_2 hydrogenation reaction, its ability to adsorb on the catalyst surface is a considerable feature for evaluating catalysts. Thus, the ability of the CO_2 molecules to chemisorb on the fabricated catalysts were assessed by TPD of CO_2; the CO_2-TPD profiles are depicted in Fig. 4. The desorption peaks centered at 100 and 155 °C could be assigned to the weak and medium chemisorption of CO_2 molecules on the catalyst supports, respectively [34, 35], which probably originated from the carbonate species interacting with the catalyst surface. Note that the intensities of these desorption peaks were dependent on the calcination condition of the Nb_2O_5, or rather, on the acidity of the catalyst. In short, the concentration of the desorbed CO_2 molecules on the catalysts, which is proportional to the peak area, exhibited an upward trend when the catalyst acidity decreased, as shown in Table 1. Moreover, the Pt/Nb_2O_5-500 and Pt/Nb_2O_5-600 catalysts possessed a higher amount of medium-chemisorbed CO_2 molecules in comparison with that from the Pt/Nb_2O_5-300 and Pt/Nb_2O_5-400 catalysts, indicating that the CO_2 molecules formed a stronger bond to the former catalysts. The observed trend and strength of the CO_2 bonds are reasonable because CO_2 is an acidic molecule, so adsorption on the surface of the highly acidic catalyst support is unfavorable. The CO_2-TPD

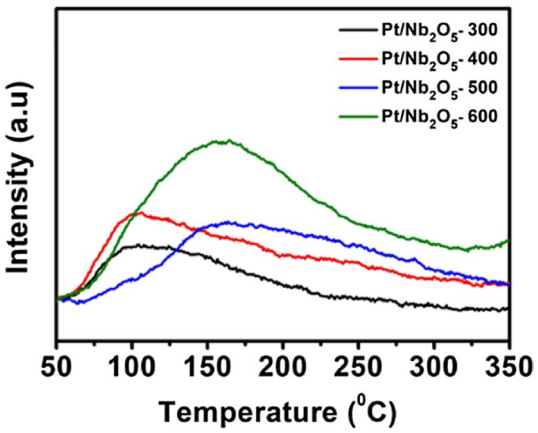

Fig. 4 CO_2-TPD evaluation of the Pt/Nb_2O_5-x catalysts at temperatures of 50–350 °C

data clearly demonstrated that CO_2 molecules preferred to adsorb on the catalyst surface with lower acidity.

The Pt-based catalysts were reduced under H_2 at 300 °C for 2 h, and the surface oxidation states of the Pt NPs in each catalyst were investigated using XPS. Before the analysis, the C 1s peak position was adjusted to 284.6 eV and all the Pt peaks were then calibrated. All the XPS spectra were fitted using the Casa XPS program, and the results are depicted in Fig. S1. The Pt 4f peaks of all the catalysts showed metallic (Pt^0) and oxidized (Pt^{2+} and Pt^{4+}) phases, in good agreement with other reports found in the literature [12, 36]. Detailed Pt^0 $4f_{7/2}$ positions for the catalysts were collected and are shown in Table 1. It is worth noting that the Pt^0 $4f_{7/2}$ peak positions of the Pt/Nb_2O_5-500 and Pt/Nb_2O_5-600 catalysts (i.e. 71.05 eV and 71.03 eV, respectively) were close to that of Pt foil (70.9 eV) [37]. However, in the Pt/Nb_2O_5-300 and Pt/Nb_2O_5-400 catalysts, this peak position shifted to higher binding energies (BE) by approximately 0.5 and 0.2 eV, respectively. The peak shift to a higher BE, meaning that the Pt surface possessed a more positive charge, is interpreted by means of the electron-poor surface of the Pt NPs because more electrons moved from the Pt to the support with more acidic sites [38, 39]. The data obtained from XPS indicated that when the acidity of the catalyst support increased, the interaction between the Pt metal and the support was strengthened. To this end, a stronger metal–support interaction partially assisted the growth of the smaller Pt NPs by preventing sintering, as reflected in the Pt size distributions of the synthesized Pt-based catalysts observed using TEM.

3.2 Catalytic Performance

Before loading the catalysts, a blank test was carried out for direct CO_2 hydrogenation to MeOH and DME from 180 to 300 °C at a pressure of 5 bar. Only the starting gases (i.e. CO_2, H_2, and N_2) and no product were detected (data were not shown), indicating that the catalysts played a critical role in commencing the reaction. When the fabricated Pt/Nb_2O_5-x catalysts were applied to the CO_2 hydrogenation reaction to MeOH and DME under the same reaction conditions, CO, MeOH, and DME were the carbon-containing products that could be detected by the TCD and FID. Generally, the CO_2 hydrogenation reaction is comprised of two main parallel reactions, namely methanol synthesis and the reverse water gas shift (rWGS). Figure 5a showed the dependence of CO_2 conversion on temperature for all the catalysts, which followed an upward trend as the reaction temperature increased. CO_2 conversion was relatively poor, with the highest value of 6% from the Pt/Nb_2O_5-300 catalyst, which was most likely because the pressure applied for the reaction was low. Furthermore, the acidity was found to promote CO_2 conversion, as depicted in Fig. 5b. The Pt/Nb_2O_5-300 and Pt/Nb_2O_5-600

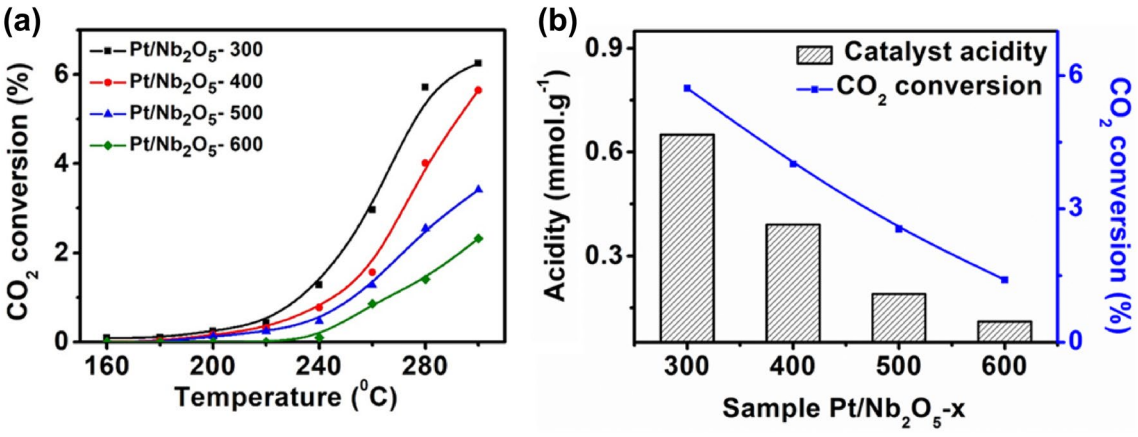

Fig. 5 **a** Dependence of CO_2 conversion on the reaction temperature for the Pt-based catalysts. **b** Dependence of CO_2 conversion on the total number of acidic sites of the Pt-based catalysts at 280 °C

catalysts, which possessed the highest and lowest acidity among the catalysts, resulted in 5.7% and 1.4% CO_2 conversion, respectively, at 280 °C. In the hydrogenation reaction, the metal active sites are a decisive factor that influence reaction conversion because they serve to dissociate the adsorbed H_2 molecules. Additionally, a low electron density on the metal surface weakens the M–H bonding, which enriches the source of H atoms needed for the hydrogenation process [38, 40]. Meanwhile, support acidity withdraws electrons from the supported metal surface and promotes metal dispersion, as was confirmed by XPS and CO chemisorption analyses of the Pt-based catalysts in this work. The Pt/Nb_2O_5-300 catalyst has the highest Pt dispersion and an electron-poor Pt surface caused by the large number of acidic sites existing on the catalyst support; therefore, the enhanced dissociation of H_2 leads to an increase in CO_2 conversion. In addition to the factors mentioned above that affect the CO_2 conversion, oxygen vacancies could be a possibility that also affects the CO_2 conversion. Generally, oxygen vacancies are widely known as sites where CO_2 molecules could be adsorbed [41]. Therefore, more oxygen vacancies can result in higher CO_2 conversion. To analyze the oxygen vacancies, Raman analysis was performed and the results are shown in Fig. S2. As shown, a broad band was observed with the band center within 650–680 cm^{-1} for the Pt-Nb_2O_5-400 and -500 catalysts. This band could be characterized as the stretching vibration modes of the octahedral structure. The large peak shift might originate from the thermal treatment of the support Nb_2O_5 at different temperatures, which resulted in a phase transformation, including the amorphous phase, as shown in the XRD results. Also, since we treated the Nb_2O_5 in air, the number of oxygen vacancies is considered to be negligible. Therefore, we can conclude that oxygen vacancies from the different calcination temperatures have little effect on the CO_2 conversion.

To obtain steady conditions for a reliable catalytic investigation, all the synthesized catalysts had to be stable during the reaction process; thus, we carried out a stability test on all the catalysts. As seen in Fig. 6, all the catalysts exhibited a constant conversion of CO_2 at 260 °C for over 2000 min, indicating that the prepared catalysts were sufficiently stable over the course of the experiment.

Figure 7a shows the turnover frequency (TOF) (top) and selectivity (bottom) of MeOH production from all the catalysts as a function of reaction temperature. The TOF were calculated with respect to the number of metallic Pt sites obtained from the CO chemisorption. All the catalysts started producing MeOH at ca. 200 °C; however, the Pt/Nb_2O_5-600 catalyst started at ca. 260 °C, probably because this sample had a large Pt particle size, which deterred the CO_2 reaction and the production of MeOH. The TOF for MeOH had a volcano-shaped figure with the top of the volcano located in the temperature range of 240–260 °C.

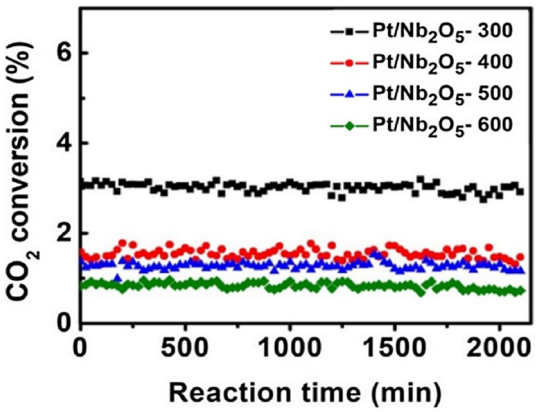

Fig. 6 Stability test for the Pt-based catalysts at 260 °C

This trend has been reported in the literature and could be explained by the thermodynamic and kinetic behaviors of the reaction [42, 43]. In the low-temperature region, MeOH formation is favorable because the reaction to produce MeOH is exothermal and more energy is required to activate the stable CO_2 molecules. When the temperature is higher, however, the formation of CO via the rWGS reaction is faster and more favorable because it is endothermic [44]. Among the catalysts, Pt/Nb_2O_5-500 possessed the highest TOF value of 0.073 s^{-1} at 260 °C, followed by Pt/Nb_2O_5-600 (TOF value of 0.070 s^{-1}) at the same temperature. On the other hand, MeOH selectivity decreased monotonically with ascending temperature, as shown in Fig. 7a (bottom), which was because the production of CO via the rWGS reaction is predominant and preferable at high temperatures. There are many factors that affect MeOH production depending on the catalytic system selected for the investigation, such as metal surface sites [45] and metal oxidation [46]. In our case, only the acidity of the support was modified while all other parameters were kept constant; therefore, MeOH production could be reasonably linked to the acidic properties of the support. Figure 7b showed the dependence of MeOH selectivity at 280 °C on the total acidity of the catalyst supports, which clearly indicated that the production of MeOH decreased with increasing support acidity. The Pt/Nb_2O_5-300 catalyst showed the lowest selectivity (0.44%) whereas Pt/Nb_2O_5-600 exhibited the highest (0.80%). When the catalyst support was enriched with acidic sites, the number of adsorbed CO_2 molecules decreased because CO_2 is an acidic molecule, which was confirmed by the CO_2-TPD data of the synthesized Pt/Nb_2O_5-x catalysts. This, in turn, could lead to a drop in the possibility to form MeOH. Furthermore, experimental studies and theoretical calculations have revealed that the adsorption structure of CO_2 molecules on an active metal surface plays a decisive role in determining MeOH formation [47–50]. Accordingly, carbon-containing intermediates induced during the course of the CO_2

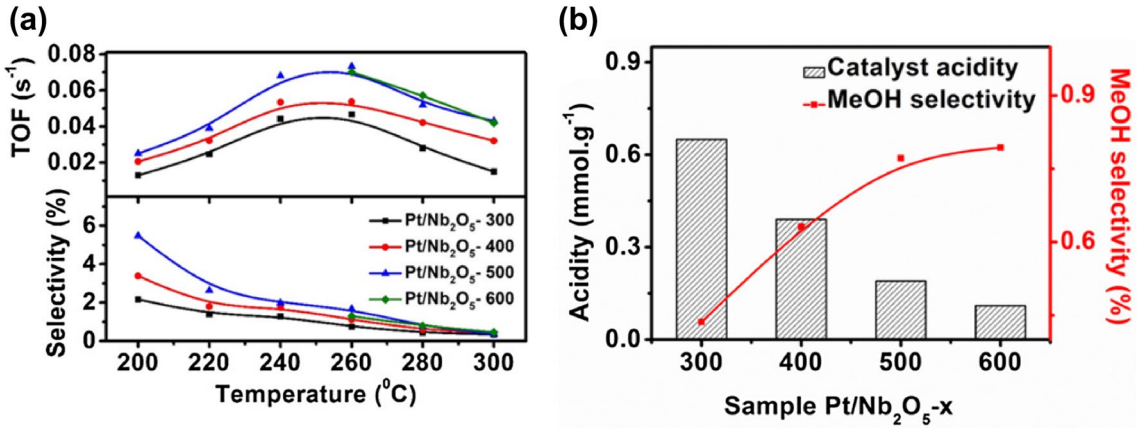

Fig. 7 Effect of reaction temperature on the **a** TOF (top) and selectivity (bottom) of MeOH for the Pt-based catalysts. **b** Dependence of MeOH selectivity on the total number of acidic sites of the Pt-based catalysts at 280 °C

hydrogenation reaction by the rWGS + CO-Hydro pathway promotes the formation of carboxylate (*HOCO) species that have been confirmed as the origin for MeOH production using Pt-based catalysts [51]. Despite the complexity of the reaction intermediates, these carbonate species have been identified using IR with bands appearing primarily in the range of 1800–1200 cm^{-1} [52, 53].

To clarify the dependence of MeOH production on the catalyst acidity obtained in this work, we carried out a DRIFT study to seek insight into the ability to form carbonaceous species on the catalyst surface during the reaction. The DRIFT measurements were performed using the Pt/Nb_2O_5-300 and Pt/Nb_2O_5-500 catalysts as representatives. The catalysts were reduced in H_2 at 300 °C for 2 h before starting CO_2 hydrogenation; IR spectra at different reaction temperatures were collected. As shown in Fig. 8, both catalysts exhibited strong bands at ca. 2060 cm^{-1}, which are attributed to linear adsorbed CO species on the Pt surface [54]. These species were formed during the catalytic reaction, and mainly contribute to the production of CO by the direct C–O cleavage pathway [51]. The evolution of this peak in both catalysts with increasing reaction temperature clearly confirmed the enrichment of the CO product at elevated temperatures. In the range of 1800–1200 cm^{-1}, however, the two catalysts showed different evolution of the spectra, suggesting a differentiation in the formation of the carbonaceous intermediates, which inevitably influenced the MeOH production. As shown in Fig. 8a, only a band with low intensity emerged at 1528 cm^{-1} when the Pt/Nb_2O_5-300 catalyst with high acidity was employed, which can be assigned to carboxylate species [55]; whereas in Fig. 8b, the Pt/Nb_2O_5-500 catalyst with low acidity exhibited a much

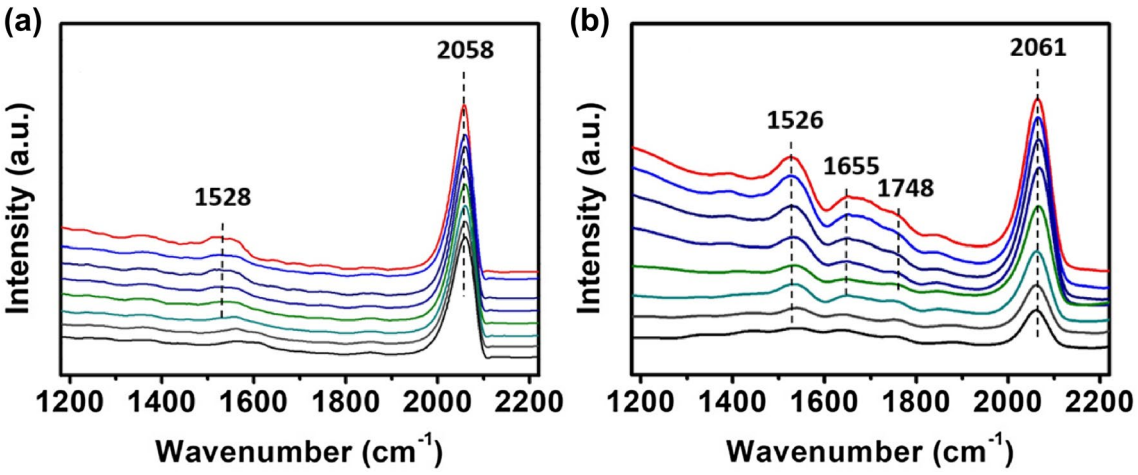

Fig. 8 Sequence of in situ DRIFT spectra obtained during linear heating (5 °C min^{-1}) at the CO_2 hydrogenation conditions on the **a** Pt/Nb_2O_5-300 and **b** Pt/Nb_2O_5-500 catalysts. Reaction temperatures (from bottom to top): 190, 200, 220, 240, 255, 270, 285, and 300 °C

higher intensity for this peak. Moreover, a peak centered at 1655 cm^{-1} could be assigned to bicarbonate species [54, 56] and another peak at 1748 cm^{-1} was attributed to bridged carbonate [57]. The data provide a direct observation that the ability to form carbon-containing intermediates on the surface of the Pt/Nb_2O_5-300 catalyst (i.e. possibly inducing MeOH production during the reaction) is less than that of the Pt/Nb_2O_5-500 catalyst, thus the Pt/Nb_2O_5-300 catalyst produced less MeOH. It is worth noting that the intensity of these peaks was minor in comparison with that of the CO linear peak, implying that the production of CO was predominant, which is consistent with the results obtained from the catalytic experiments. Apart from that, other IR bands of both catalysts had significantly low intensities; thus, detailed identification and interpretation were not attempted. The data obtained from the CO_2-TPD analysis, the catalytic experiments, and the DRIFT study certainly demonstrated that CO_2 molecules unfavorably adsorbed and indeed, formed carbon-containing species on the catalyst surface with high acidity, leading to the decrease in MeOH production.

CO_2 hydrogenation to produce DME consists of two processes: MeOH is first formed from the hydrogenation of CO_2 in the presence of metallic catalysts, followed by its dehydration to produce DME with the assistance of acid catalysts [19]. As seen in Fig. 9a, all the catalysts showed a downward trend for DME selectivity when the reaction temperature increased, which was caused by the dominance of CO selectivity produced from rWGS at high temperature. In addition, because the dehydration of MeOH to DME is an exothermic reaction, the production of DME is only favored at low reaction temperatures [58]. Furthermore, since DME was directly produced from MeOH which formed during the reaction, the production of MeOH is crucial to control DME selectivity. However, MeOH selectivity decreased with increasing reaction temperature, as observed in Fig. 7a (bottom), which contributed to the drop in DME selectivity to some extent. There have been several mechanisms proposed for the dehydration of MeOH to DME, and acidity is well accepted to be responsible for the formation of carbonaceous intermediates, which in turn result in the promotion of DME [59, 60]. The Pt/Nb_2O_5-300 and Pt/Nb_2O_5-400 catalysts started producing DME at 200 °C, while Pt/Nb_2O_5-500 started at 260 °C, and Pt/Nb_2O_5-600 did not produce DME, which was most likely due to its extremely low number of acidic sites. Among the catalysts, Pt/Nb_2O_5-300 exhibited the highest DME selectivity over the course of the reaction, and the highest value in this catalyst was 2.6% at 200 °C. Figure 9b showed DME selectivity at 280 °C as a function of catalyst support acidity, which demonstrated that the catalyst having a higher support acidity produced more DME. Accordingly, the Pt/Nb_2O_5-300, Pt/Nb_2O_5-400, and Pt/Nb_2O_5-500 catalysts corresponded to DME selectivities of 0.74, 0.59, and 0.37%, respectively. These results further verified the advantage of using catalysts with acidic properties to improve the performance of CO_2 hydrogenation to DME.

4 Conclusions

The impact of acidity on the direct hydrogenation of CO_2 to MeOH and DME was examined using Pt supported on Nb_2O_5. The number of acidic sites of the metal oxide supports was controlled by employing different calcination temperatures, and Pt NPs were grown on the acidic sites via the impregnation method. The acidity was found to enhance the metal–support interaction and metal dispersion, resulting in the improvement of CO_2 conversion. The increase in support acidity was detrimental for the production of MeOH

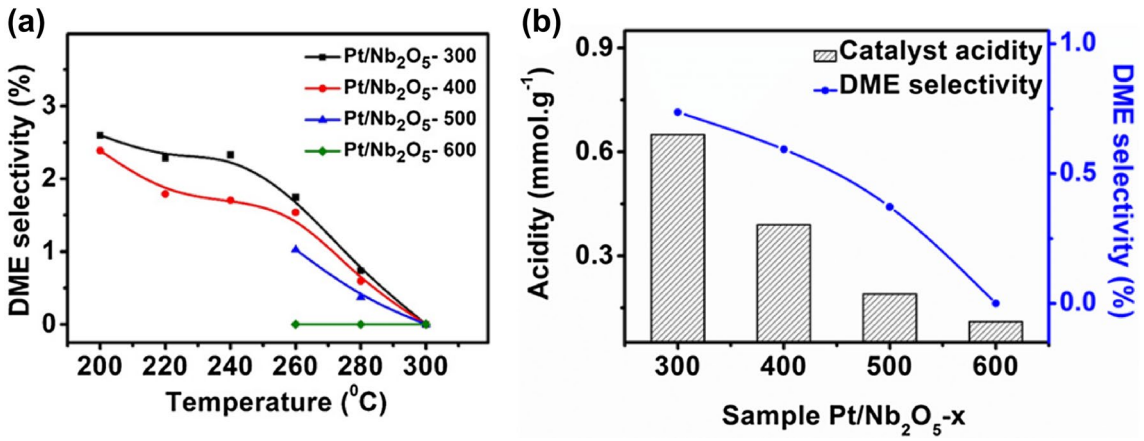

Fig. 9 **a** Effect of reaction temperature on DME selectivity for the Pt-based catalysts. **b** Dependence of DME selectivity on the total number of acidic sites on the Pt-based catalysts at 280 °C

because of the decrease in carbon-containing intermediates formed from adsorbed CO_2 molecules on the surface of the catalysts, as demonstrated by our in situ DRIFT study. In contrast, DME production was enhanced when the support acidity increased, with the Pt/Nb_2O_5-300 catalyst exhibiting the highest selectivity of 2.6% at 200 °C, confirming the advantage of acidity in the production of DME.

Acknowledgements This work was supported by the Institute for Basic Science (IBS) [IBS-R004].

Compliance with Ethical Standards

Conflict of interest The authors report no conflict of interest.

References

1. Park JY, Somorjai GA (2016) Catal Lett 146:1
2. Gupta P, Paul S (2014) Catal Today 236:153
3. Tanabe K, Hölderich WF (1999) Appl Catal A 181:399
4. Hattori H (2015) Appl Catal A 504:103
5. Park JY, Baker LR, Somorjai GA (2015) Chem Rev 115:2781
6. Kim SM, Lee SW, Moon SY, Park JY (2016) J Phys Condens Matter 28:254002
7. Na K, Alayoglu S, Ye R, Somorjai GA (2014) J Am Chem Soc 136:17207
8. Silva A, Wilson K, Lee AF, Dos Santos VC, Cons Bacilla AC, Mantovani KM, Nakagaki S (2017) Appl Catal B 205:498
9. Nakajima K, Baba Y, Noma R, Kitano M, Kondo JN, Hayashi S, Hara M (2011) J Am Chem Soc 133:4224
10. Ziolek M, Sobczak I (2017) Catal Today 285:211
11. Tanabe K, Okazaki S (1995) Appl Catal A 133:191
12. Moon SY, Naik B, Jung C, Qadir K, Park JY (2016) Catal Today 265:245
13. Park D, Kim SM, Kim SH, Yun JY, Park JY (2014) Appl Catal B 480:25
14. Jehng JM, Wachs IE (1991) J Phys Chem 95:7373
15. Nico C, Monteiro T, Graça MPF (2016) Prog Mater Sci 80:1
16. Murayama T, Chen J, Hirata J, Matsumoto K, Ueda W (2014) Catal Sci Technol 4:4250
17. Tanabe K (1987) Mater Chem Phys 17:217
18. Riaz A, Zahedi G, Klemeš JJ (2013) J Clean Prod 57:19
19. Bakhtyari A, Rahimpour MR (2018) Chapter 10—methanol to dimethyl ether. In: Dalena F (ed) Methanol. Elsevier, Amsterdam, p 281
20. Zhong C, Guo X, Mao D, Wang S, Wu G, Lu G (2015) RSC Adv 5:52958
21. Guo X, Mao D, Lu G, Wang S, Wu G (2011) J Mol Catal A 345:60
22. Gao P, Li F, Zhan H, Zhao N, Xiao F, Wei W, Zhong L, Wang H, Sun Y (2013) J Catal 298:51
23. Hengne A, Bhatte KD, Ould CS, Saih Y, Basset JM, Huang KW (2018) ChemCatChem 10:1
24. Silva RJ, Pimentel AF, Monteiro RS, Mota CJA (2016) J CO2 Util 15:83
25. Gnanakumar ES, Chandran N, Kozhevnikov IV, Grau-Atienza A, Fernandez EVR, Sepulveda-Escribano A, Shiju NR (2019) Chem Eng Sci 194:2
26. Porosoff MD, Yan B, Chen JD (2016) Energy Environ Sci 9:62
27. Wang W, Wang S, Ma X, Gong J (2011) Chem Soc Rev 40:3703
28. Oh S, Back S, Doh WH, Moon SY, Kim JJ, Park JY (2017) RSC Adv 7:45003
29. Bonura G, Cordaro M, Spadaro L, Cannilla C, Arena F, Frusteri F (2013) Appl Catal B 140–141:16
30. Sousa LFD, Toniolo FS, Landi SM, Schmal M (2017) Appl Catal A 537:100
31. Hernández MC, Otter HD, Weber JL, De Jong KP (2017) Appl Catal A 548:143
32. Graça MPF, Meireles A, Nico C, Valente MA (2013) J Alloys Compd 553:177
33. Trung TSB, Kim Y, Kang S, Kim S, Lee H (2015) Appl Catal A 505:319
34. Li L, Wen X, Fu X, Wang F, Zhao N, Xiao F, Wei W, Sun Y (2010) Energy Fuels 24:5773
35. Wang F, Xu L, Shi W, Zhang J, Wu K, Zhao Y, Li H, Li HX, Xu GQ, Chen W (2017) Nano Res 10:364
36. Trung TSB, Choi HS, Oh S, Moon SY, Park JY (2018) RSC Adv 8:21528
37. Briggs D (1979) Handbook of X-ray photoelectron spectroscopy. Elsevier, Woodbury
38. Crampton AS, Rötzer MD, Landman U, Heiz U (2017) ACS Catal 7:6738
39. Ramaker DE, De Graaf J, Van Veen JAR, Koningsberger DC (2001) J Catal 203:7
40. Wang Z, Kim KD, Zhou C, Chen M, Maeda N, Liu Z, Shi J, Baiker A, Hunger M, Huang J (2015) Catal Sci Technol 5:2788
41. Pan Y, Liu C, Mei D, Ge Q (2010) Langmuir 26:5551
42. Guo X, Mao D, Lu G, Wang S, Wu G (2010) J Catal 271:178
43. Díez-Ramírez J, Sánchez P, Rodríguez-Gómez A, Valverde JL, Dorado F (2016) Ind Eng Chem Res 55:3556
44. Centi G, Perathoner S (2009) Catal Today 148:191
45. Fujita SI, Moribe S, Kanamori Y, Kakudate M, Takezawa N (2001) Appl Catal A 207:121
46. Toyir J, Ramírez de la Piscina P, Fierro JLG, Homs NS (2001) Appl Catal B 34:255
47. Taylor PA, Rasmussen PB, Chorkendorff I (1995) J Chem Soc Faraday Trans 91:1267
48. Yoshihara J, Parker SC, Schafer A, Campbell CT (1995) Catal Lett 31:313
49. Fujitani T, Nakamura I, Uchijima T, Nakamura J (1997) Surf Sci 383:285
50. Grabow LC, Mavrikakis M (2011) ACS Catal 1:365
51. Pozdnyakova O, Teschner D, Wootsch A, Krohnert J, Steinhauer B, Sauer H, Toth L, Jentoft FC, Knop-Gericke A, Paal Z, Schlogl R (2006) J Catal 237:1
52. Sápi A, Halasi G, Kiss J, Dobó DG, Juhász KL, Kolcsár VJ, Ferencz Z, Vári G, Matolin V, Erdőhelyi A, Kukovecz A, Kónya Z (2018) J Phys Chem C 122:5553
53. Arunajatesan V, Subramaniam B, Hutchenson KW, Herkes FE (2007) Chem Eng Sci 62:5062
54. Raskó J (2003) J Catal 217:478
55. Wang X, Hong Y, Shi H, Szanyi J (2016) J Catal 343:185
56. Baltrusaitis J, Schuttlefield J, Zeitler E, Grassian VH (2011) Chem Eng J 170:471
57. Wachs IE (1995) Colloid Surf A 105:143
58. Azizi Z, Rezaeimanesh M, Tohidian T, Rahimpour MR (2014) Chem Eng Process 82:150
59. Kubelková L, Nováková J, Nedomová K (1990) J Catal 124:441
60. Bandiera J, Naccache C (1991) Appl Catal 69:139

Affiliations

Si Bui Trung Tran[1] · Hanseul Choi[1,2] · Sunyoung Oh[1,2] · Jeong Young Park[1,2]

✉ Jeong Young Park
jeongypark@kaist.ac.kr

[1] Center for Nanomaterials and Chemical Reactions, Institute for Basic Science (IBS), Daejeon 305-701, Republic of Korea

[2] Department of Chemistry and Graduate School of EEWS, Korea Advanced Institute of Science and Technology (KAIST), Daejeon 305-701, Republic of Korea